PCCP

Accepted Manuscript

ROYAL SOCIETY OF CHEMISTRY

www.rsc.org/pccp

Long term puzzles of the CH and CD energetics and related phenomena revisited; Solutions sought through REMPI-photofragmentations of bromomethanes

Arnar Hafliðason, Huasheng Wang, and Ágúst Kvaran*
Science Institute, University of Iceland, Dunhagi 3, 107 Reykjavík, Iceland.

Total number of pages in manuscript: 34
Tables: 4
Figures: 6
"RBr-CH-CD-REMPI-r.docx"

*Correspondence should be addressed to:

Agust Kvaran
Permanent address:
Science Institute,
University of Iceland,
Dunhagi 3, 107 Reykjavík,
Iceland
Phone: +354-525-4672 (A.K. office)
Phone: +354-525-4800 (main office)
URL: https://www.hi.is/~agust/
E-mail: agust@hi.is

Abstract

Ever since the pioneering work by Herzberg and Johns in 1969 (The Astrophysical Journal. **158**, 399, (1969)) the spectral assignment and the energetics of the fundamental molecular fragment CH, in the region of 63 000 – 65 000 cm^{-1} (7.81 – 8.06 eV), has remained a puzzle to large extent. Dissociation of bromoform and deuterated bromoform following two-photon resonance excitations to molecular Rydberg states form the fragment species CH* and CD* in the excited state $A^2\Delta(v'=0)$ as well as carbon and bromine atoms in the ground and first excited states, C/C* and Br/Br*. Further (1_r+1_i)REMPI of CH* and CD* resonance excites the fragments to the energy region of concern, whereas the atom fragments were identified by further $(2_r + 1_i)$REMPI. Analysis based on spectral simulations, isotope shifts and comparison with others data allowed spectral identifications, assignments and partial characterization of four highly excited bound states for each of the molecular fragments (CH**/CD**); including the $(3)^2\Pi$ valence state and the $(4)^2\Pi$ Rydberg state, for the first time. Perturbations, showing as line-shifts, line-intensity and/or line-width alterations, due to level-to-level state interactions between the bound states and predissociations by a repulsive state are recognized. Recording of C^+ signals in REMPI of several bromomethanes for one-photon energy of about 40 333 cm^{-1} allows clarification of a mystery concerning a broad C^+ band frequently observed. The work, presented, demonstrates the usefulness of molecular REMPI for fragment analysis.

INTRODUCTION

The spectroscopy and photofragmentation of the bromomethanes, CH_xBr_{4-x}, (x = 0 – 3) has been studied both experimentally and theoretically for decades.[1-14] Whereas, most of the studies concern the lower energy valence states, limited information are available relevant to higher energy Rydberg states. In addition to being of interest for fundamental studies, the compounds and their photofragmentation species are of importance both in atmospheric chemistry and astrochemistry.[15-21] Thus, photofragmentation processes have been of interest

due to bromine atom formation and its ozone depletion effects [3, 4, 11-13, 22, 23] in the atmosphere and because CH_n (n = 1-3) radicals and the corresponding ions are believed to be fundamental building units for formation of bigger organic molecules in the interstellar space.[19, 24]

Standard UV absorption spectra of the bromomethanes reveal transitions to repulsive valence states corresponding to $\sigma^* \leftarrow$ nb transitions in the near-UV region of about 180 – 290 nm [1, 23, 25, 26] and transitions to Rydberg states in the far-UV region of about 110 – 180 nm.[10, 13, 14, 27, 28] REMPI spectra of CH_3Br [10, 13] and CH_2Br_2 [14] show structure due to transitions to Rydberg states. Generally, less clear Rydberg state progressions are seen as the number of bromine atoms increases. Photodissociation processes, via Rydberg states, are believed to form atoms and molecular fragments such as Br, CH and C in ground and excited (Br*, CH* and C*) states. Fig. 1 shows some $(2_r + m_{r,i})$REMPI processes for CH_xBr_{4-x}, (x = 2, 3), where 2_r refers to two-photon resonance excitation of the parent molecule and $m_{r,i}$ refers to further m photons required for resonance and/or ionization excitations. The fragment ions can be formed by further resonance or non-resonance excitations of the neutral fragments. Thus, for example, the atom ions (Br^+, C^+) and CH^+ can be formed by further $(2_r + 1_i)$ and $(1_r + 1_i)$ REMPI, respectively, in which case m_{ri} are $(2_r + 1_i)$ and $(1_r + 1_i)$, respectively. Therefore, the REMPI ion signals can both reflect the parent molecular spectral structure as well as that of the fragments.

The CH radical is a fundamental unit for possible photoassisted formation of organic molecules in interstellar space. Therefore, its high energy electronic states are of great astrochemical interest. Since the UV and VUV spectroscopic studies of the CH radical by Herzberg and Johns in 1969 [29] there have been a number of conflicts and unsolved puzzles concerning its spectral assignments in the high energy Rydberg state region. Herzberg and Johns assigned spectra with the band origins 58 981, 64 212 and 64 531 cm^{-1} to transitions from the ground state ($X^2\Pi(v'' = 0)$) to the $D^2\Pi(v' = 0)$, $E^2\Pi(v' = 0)$ and $F^2\Sigma^+(v' = 0)$ states,

respectively. Later P. Chen *et al*. assigned a spectrum recorded by the multiphoton ionization technique at 64 150 cm^{-1} to the upper state $D^2\Pi(v'= 2)$, whereas a spectrum near 63 000 cm^{-1} was assigned to a $^2\Sigma^+$ upper state (labeled as $E'^2\Sigma^+$). [30, 31] Three bound $^2\Pi$ states and one $^2\Sigma$ state, close in energy, were predicted to be found in this region according to *ab initio* calculations.[32, 33] Tjossem and Smyth noticed unusual rotational line intensities in the two-photon REMPI spectrum of CH due to the $D^2\Pi(v'= 2) \leftarrow\leftarrow X^2\Pi(v''= 0)$ resonance transition because of near-resonance with the intermediate $C^2\Sigma^+$ $(v'= 0)$ state,[34] resulting in enhanced line intensities in the *Q* branch for rotational quantum numbers close to $N = 8$. This was further verified by Wang *et al.*, who also noticed a sudden onset of predissociation for $N \geq 12$, which they attributed to complex interactions among $^2\Pi$ states, close in energy, in that region.[35] In 2000 Y. Chen *et al.* published a CH REMPI spectrum with number of rotational lines detected for multiphoton ionization of $CHBr_3$ in argon which they assigned to the single-photon resonance transition $CH^{**}(D^2\Pi(v'= 2)) \leftarrow CH^*(A^2\Delta(v'= 0))$ with band origin of 40 991.5 cm^{-1}.[36] Recently J. Long *et al*. detected CH bands in the same energy region (40 550 – 41 250 cm^{-1}) in REMPI spectra of CH_2Br_2.[14] Less extensive rotational structure, compared to that observed for $CHBr_3$, associated with different exothermicity in photodissociation channels, allowed identification of three different electronic transitions from the $A^2\Delta(v'= 0)$ state with band origins of 40 762, 40 991.5 and 41 155 cm^{-1}. These were assigned to transitions to the CH**(Fig. 1) states $E^2\Pi(v'= 0)$, $D^2\Pi(v'= 2)$ and $F^2\Sigma^+(v'= 0)$, respectively. Observation of the forbidden $F^2\Sigma^+(v'= 0) \leftarrow A^2\Delta(v'= 0)$ transition was explained as being due to an enhanced transition probability gained by mixing with nearby states.

Different interpretations of broad C^+ ion peaks, observed in REMPI of $CHBr_3$,[36] CH_2Br_2[14] and CH_3Br,[13] for a one-photon wavenumber of about 40 333 cm^{-1}, remain in the literature, without clear confirmations. Y. Chen *et al*. attributed the peak to a one-photon resonance excitation of $CH^*(A^2\Delta(v'= 0))$ to a short lived, predissociating, bound state,

CH**($(3)^2\Pi(v' = 0)$) followed by photodissociation to form C^+ and H via two-photon excitation to a repulsive CH^+ state.[36] The lifetime of the intermediate state, ($(3)^2\Pi(v' = 0)$), was believed to be very short due to predissociation by a repulsive $^2\Pi$ state to form C*($^1D_2$) and H.[32] Long *et al*.,[14] on the other hand, suggest that the peaks are due to intensity enhancements in the REMPI of the molecules in the case of C^+ formation because of an increased transition probability by switching from three-photon to two-photon non-resonance ionization of C*($^1D_2$).

Large number of bromine atomic lines, due to ($2_r + 1_i$)REMPI of the ground (Br) and spin-orbit excited (Br*) species, are observed in REMPI of CH_3Br[13] and CH_2Br_2.[14] The Br and Br* species are believed to be partly formed by one-photon photodissociation via excitations to repulsive molecular valence states and partly due to predissociation of the parent molecular Rydberg states following two-photon excitation (See Fig. 1).

In this paper we present and analyse mass resolved REMPI data of bromoform, for two-photon excitation to a high energy Rydberg state region. The data show a) -broad spectral features due to excitations to molecular Rydberg states, b) -carbon and bromine atomic spectra as well as c) -spectra due to resonance transitions from CH*$A^2\Delta$. The mystery concerning the nature of the broad C^+ peak, seen in REMPI of number of bromomethanes, mentioned above, for one-photon excitation of about 40 333 cm^{-1}, is clarified. A special focus is on the energetics and nature of electronic states of CH** in the energy region of 63 000 – 65 000 cm^{-1} (7.81 – 8.06 eV), which has been a puzzle for decades (see above). Simulation based analysis of the CH*($A^2\Delta$ ($v' = 0$)) spectra as well as the corresponding spectra for CD* derived from REMPI of $CDBr_3$ allow clarification of the highly mixed electronic states in that region as well as the relevant spectroscopy.

EXPERIMENTS

The equipment used in the experiments is similar to what has been described before.[37-39] Mass spectra were recorded as a function of laser excitations for various bromomethanes corresponding to two-photon excitation of 76 000 – 84 000 cm^{-1} / one photon excitation of 38 000 – 42 000 cm^{-1}. A Coherent ScanMatePro dye laser was pumped by a XeCl (308 nm) excimer laser from Lamda Physics (COMPex 205) at a repetition rate of 10 Hz. Outputs for the dyes C-503 and C-480, frequency doubled by a BBO crystal (SHG-215 from Sirah) were used to cover the wavelength range of concern (238 – 263 nm). The bandwidth of the dye laser beam was about 0.095 cm^{-1}. Typical laser intensities used were about 0.1 – 0.3 mJ/pulse. Argon gas was swept over samples of liquids ($CHBr_3$ (Acros Organics; purity 96%),$CDBr_3$ (Sigma Aldrich; purity 99.5%) and CH_2Br_2 (Merck Schuchardt; purity 98%)) and solids (CBr_4 (Acros Organics; purity 98%)), kept in a trap at room temperature for total pressure of about 1.0 bar, whereas a sample of pure CH_3Br gas (Merck Schuchardt; purity 99.5%) at about 1.0 to 1.5 bar was used. Samples were let through a pulsed nozzle (500 μm) into an ionization chamber. The pressure in the ionization chamber was kept lower than 10^{-6} mbar during experiments. The nozzle was kept open for about 200 – 400 μs, and the laser beam was fired about 450 – 500 μs after the nozzle was opened. Ions formed were extracted into a 0.75 meter long time-of-flight tube and detected by MCP plates. Signals were fed into a LeCroy WaveSurfer 44MXs-A 400 MHz storage oscilloscope. Signal levels were recorded for a fixed number of 50 laser pulses, for laser wavenumber steps of 0.1 or 0.2 cm^{-1} to give mass resolved REMPI data. REMPI spectra were obtained by integrating signals for a particular mass as a function of laser excitation wavenumber. Saturation and power broadening was avoided by minimizing laser power. Laser calibration was based on observed ($2_r + 1_i$)REMPI halogen atomic lines. The accuracy of the calibration was found to be about ± 2.0 cm^{-1} on the two-photon scale. Overall spectra were constructed of smaller scans which were normalized to

each other by using intensities of band that are common to neighbouring sections.

RESULTS AND DISCUSSION

REMPI spectra main features and interpretations

Mass resolved ($2_r + m_{r,i}$)REMPI data were collected for $CHBr_3$ for the two-photon excitation region of 76 000 – 84 000 cm^{-1} (one-photon excitation region of 38 000 – 42 000 cm^{-1}). Only the C^+, CH^+ and $^iBr^+$ (i = 79,81) fragment ions were detected. Fig. 2(a) shows the relevant REMPI spectra along with the one-photon absorption spectrum.[1] Narrow and sharp peaks detected in the atom fragment spectra (C^+ and Br^+) are assigned to ($2_r + 1_i$) REMPI of C/C* and Br/Br*.[40] Majority of the peak structure detected in the region of 80 760 – 82 300 cm^{-1} for CH^+ is assigned to REMPI of CH*($A^2\Delta$(v′= 0)). The broad peak at 80 666 cm^{-1}, detected in the C^+ spectrum (also seen in the CH^+ spectrum) is attributed to an enhanced photoionization probability associated with switching from three-photon to two-photon ionization of C*($^1D_2$) (see below). Judging from the one-photon absorption spectrum of $CHBr_3$, which has been interpreted as being due to transitions to Rydberg states (Fig. 2(a)),[1] the remaining, underlying broad features of the REMPI spectra, largely similar in shape for the three spectra, are likely to be indicative of resonance transitions to parent molecular Rydberg states; its broad structure being due to short lifetimes of the states. Detected fragments, most likely, are formed by dissociation of the parent molecular excited Rydberg and valence states. Individual REMPI spectra will now be discussed in more detail.

C/C* REMPI

Energetically, the ground state C($^2P_{0,1,2}$) and the excited states C*($^1D_2$) and C*($^1S_0$), can be formed along with some of the fragments Br/Br*, CH*($A^2\Delta$), HBr and Br_2 for the two-photon excitation region of concern (76 000 – 84 000 cm^{-1}) as listed in Table 1. Ionization of these carbon atom fragments would require further two to three photons (see Fig. 3). Number of ($2_r + 1_i$)REMPI lines are observed for C($^2P_{0,1,2}$) and C*($^1D_2$) as well as one ($1_r + 1_i$)REMPI line for C*($^1S_0$).[40] Most probably majority of the detected C/C* fragments are formed by two-photon photodissociation of the parent molecule along with the other fragment species, listed in Table 1, for the lowest energy thresholds.

The broad peak at 80 666 cm^{-1} in the C^+ spectrum has also been seen in our REMPI studies of CH_3Br[13] and CH_2Br_2[14] (see Fig. 4) and by Y. Chen *et al*. for $CHBr_3$.[36] Whereas, Y. Chen *et al*. attributed the peak to ($1_r + 2_i$)REMPI of CH*($A^2\Delta$) via the short lived CH**($(3)^2\Pi(v' = 0)$) resonance state [36] an alternative explanation was given by J. Long *et al*., who suggested that it might be attributed to an enhanced photoionization probability.[14] REMPI scans of $CDBr_3$ and CBr_4 both reveal broad peaks for C^+ in the same position and analogous in shape to those recorded for the CH_xBr_{4-x} (x = 1 - 3), just above the threshold for two-photon ionization of C*($^1D_2$) (80 625.27 cm^{-1}) (see Fig. 4). This clearly indicates that the peak does not have to be associated with CH/CH* excitation. Instead we conclude that the peak is due to an enhanced non-resonance photoionization probability associated with switching from three-photon to two-photon ionization of C*($^1D_2$) formed by two-photon dissociation of the parent molecule(s). The corresponding, lower intensity, CH^+ peak (Fig. 2) is due to a Coulomb broadening of the C^+ mass signal.

Br/Br* REMPI

The bromine atomic lines, observed (Fig. 2 (a), supporting info[40]) could partly be due to a (2_r + 1_i)REMPI of bromine atoms formed by one-photon photodissociation via excitation to repulsive molecular valence states, since a one-photon excitation corresponds to the low energy tail of the weak absorption band in the near-UV spectral region [1, 41] (see Fig. 3). Considering, however, number of observations for photofragmentation via Rydberg states, these must also be, partly, due to REMPI of bromine atoms formed by predissociation of Rydberg states following two-photon excitation.[13, 14, 42, 43] Energetically, a number of bromine atom formation channels following two-photon excitation to Rydberg states could be involved (see Table 1), of which the simplest channel, involving only single-bond breaking, is likely to be dominant. Generally, lines due to transitions from ground state Br($^2P_{3/2}$) are found to be more intense than those due to transitions from the spin-orbit excited Br*($^2P_{1/2}$)[40] (Fig. 2 (a)), suggesting that dissociative channels forming ground state Br are more favourable.

CH* /CD* REMPI

A weak CH^+ REMPI spectral structure (Figs. 2 (a) and 2 (b)) observed in the two-photon excitation region of 80 760 – 82 300 cm^{-1} (one-photon excitation region of 40 380 – 41 150 cm^{-1}) resembles that observed by Y. Chen *et al*.[36] who attributed it to a (1_r + 1_i)REMPI of CH*($A^2\Delta$(v′= 0)), due to a one-photon resonance transition to the CH**((2)$D^2\Pi$(v′= 2)) state. Peaks were assigned to *P*, *Q* and *R* rotational lines. Based on simulation calculations (Fig. 2 (c)) we have reassigned the rotational line series (Table 2 (a)) as well as re-evaluated relevant spectroscopic constants for the CH**((2)$D^2\Pi$(v′= 2)) state (Tables 3 and 4). Splitting of rotational peaks, corresponding to the F_1 (CH**((2)$D^2\Pi$; Ω = 3/2) ← CH*($A^2\Delta$; Ω = 5/2)) and F_2 (CH**((2)$D^2\Pi$; Ω = 1/2) ← CH*($A^2\Delta$; Ω = 3/2)) transitions are not clearly seen due to

large spectral linewidths (4 – 6 cm^{-1}), hence short lifetimes. Resolved rotational peaks, observed for high rotational quantum numbers of the *P* line series, in particular, and positions of bandheads for individual line series formed the basis of the simulation. To approach the observed relative line intensities, a non-Boltzmann distribution needed to be assumed. Nevertheless, some broad spectral features seen in the high excitation region of the *P*, *Q* and *R* line series (two-photon excitation region of above 81 800 – 82 150 cm^{-1}) could not be reproduced by the simulation.

Energetically CH*($A^2\Delta$(v′= 0)) can be formed by two-photon-dissociation of $CHBr_3$ along with a ground state bromine molecule (Br_2) and Br or Br*, within the two-photon excitation region of concern (76 000 – 84 000 cm^{-1}) (see Table 1 and Fig. 3). Furthermore, as shown in Fig. 3, CH*($A^2\Delta$(v′= 0)) should be detectable by ($1_r + 1_i$)REMPI, via resonance excitation to CH**((2)$D^2\Pi$(v′= 2)), within the same excitation region. Thus, the overall process could be (2_r +($1_r + 1_i$))REMPI (see INTRODUCTION). Slope values of between 1.4 and 2.0 were derived from log-log plots of CH^+ peak signals vs. laser power, which is what might be expected in the case when the first resonance step (2_r) is saturated.[13, 44-46] Analogous laser power dependence observed for peaks which belong to the CH**((2)$D^2\Pi$(v′= 2)) ← CH*($A^2\Delta$(v′= 0)) resonance transitions (two-photon excitation region below 81 800 cm^{-1}) and those which could only partly be assigned to that transition (see above) makes us believe that the total peak structure corresponds to ($1_r + 1_i$)REMPI of CH*($A^2\Delta$(v′= 0)), but involving different resonance excited states, CH**.

Table 4 lists bound CH** states which have been reported experimentally and theoretically in the energy region of concern, which corresponds to a one-photon excitation from CH*($A^2\Delta$(v′= 0)) within the range 38 000 – 42 000 cm^{-1} or excitation from CH($X^2\Pi$(v′= 0)) within 61 174 – 65 174 cm^{-1}.[14, 29-31, 34-36, 47] Theoretically, three diabatic bound $^2\Pi$

potentials (labelled as (2)$D^2\Pi$, (3)$^2\Pi$ and (4)$^2\Pi$)[33] and one diabatic bound (3)$^2\Sigma^+$ potential are predicted to be found in this region (See Fig. 5). Furthermore, a repulsive $^2\Pi$ potential, cutting through the bound states to cause a complicated structure of avoided crossings is also to be expected (Fig. 5). The CH**((2)$D^2\Pi$) state, with the electron configuration of $2s\sigma^2 2p\pi^3$ at short internuclear distance is lowest in energy, whereas the rest of the bound states ((3)$^2\Pi$ ($2s\sigma^2 2p\sigma^1 2p\pi^1 2p\sigma^{*1}$), (4)$^2\Pi$ ($2s\sigma^2 2p\sigma^2 3p\pi^1$) and (3)$^2\Sigma$ ($2s\sigma^2 2p\sigma^2 3p\sigma^1$)) are all predicted to be very close in energy to make the v′= 2 level of the (2)$D^2\Pi$ state close in energy to the v′= 0 levels of the others. Experimentally, the energy of the (2)$D^2\Pi$(v′= 2) state has been found to be 40 991.5 cm^{-1}, with respect to excitation from the $A^2\Pi$ state (marked as ν^0 in Tables 3 and 4), corresponding to 64 165 cm^{-1} with respect to excitation from the $X^2\Pi$ state (i.e., $T_{v',0}$ in Tables 3 and 4).[14, 36] Herzberg and Johns [29] argued that $T_{v',0}$ = 64 531.5 cm^{-1} for the (3)$^2\Sigma^+$ state (hence ν^0 = 41 314 cm^{-1}) and recently Long *et al.*[14] reported two states at ν^0 = 40 762 cm^{-1} ($T_{v',0}$ = 63 935 cm^{-1}) and ν^0 = 41 155 cm^{-1} ($T_{v',0}$ = 64 328 cm^{-1}) as possible candidates for the $^2\Pi$ and $^2\Sigma$ states, respectively. All in all, therefore, we might expect to see spectral line structures due to transitions from CH*($A^2\Delta$(v′= 0)) to four electronic states, i.e., the (2)$D^2\Pi$(v′= 2), (3)$^2\Pi$(v′= 0), (4)$^2\Pi$(v′= 0) and (3)$^2\Sigma^+$(v′= 0) states. Whereas the short range electron configurations suggest that only the states (2)$D^2\Pi$(v′= 2) ($2s\sigma^2 2p\pi^3$) and (3)$^2\Pi$(v′= 0) ($2s\sigma^2 2p\sigma^1 2p\pi^1 2p\sigma^{*1}$) can be accesses by one-photon absorption and one-electron transfers, from the $A^2\Delta$(v′= 0) ($2s\sigma^2 2p\sigma^1 2p\pi^2$) state, mixing of states at longer ranges will allow transitions to the other states to occur.[32, 33] Transition probabilities, hence relative spectral intensities, however, are likely to differ largely. Thus, one might expect, the spectrum due to the two-electron transfer, $\Delta\Lambda$ = 2, transition, (3)$^2\Sigma^+$ ($2s\sigma^2 2p\sigma^2 3p\sigma^1$) ← $A^2\Delta$ ($2s\sigma^2 2p\sigma^1 2p\pi^2$), in particular, to be very weak. Furthermore, the, apparently, large state interactions and possible predissociation processes by the repulsive $^2\Pi$ state is likely to appear

as perturbation effects in the spectra, as spectral line shifts as well as line intensity and/or as linewidth alterations.[42, 48-54]

Close look at the one-photon spectral region of about 41 290 – 41 350 cm^{-1} revealed some very weak, but reproducible, irregular structure with a prominent peak at about 41 314 cm^{-1} (Fig. 2 (b)). Comparison with the data given by Herzberg and Johns for the $(3)^2\Sigma^+(v'= 0) \leftarrow X^2\Pi(v'= 0)$ transition [29] (See Table 4), makes us assign it to the transition $(3)^2\Sigma^+(v'= 0) \leftarrow A^2\Delta(v'= 0)$. The apparently overlapping spectral structure, to be seen in the CH^+ spectrum in the one-photon spectral region of about 40 900 – 41 100 cm^{-1} (see # markings in Fig. 2 (c)), on the other hand, is too broad and unstructured in order to be able to make any sensible assignments. As an attempt to clarify the energetics of CH further, as well as to explore the corresponding energetics for CD, the CD^+ REMPI signal for $CDBr_3$ in the same energy region was recorded. The additional clarification of the CH energetics was sought through isotope shift effects as well as spectral structure differences.

The difference in the band origin ($\Delta\nu^0$) of the two isotopologues C^iH (i = 1,2), i.e., the isotope shift, can be estimated from known vibrational constants of the electronic states of concern of either of the isotopologues (i = 1 or 2) (i.e., $\omega_e'(i)$, $\omega_e x_e'(i)$, $\omega_e''(i)$ and $\omega_e x_e''(i)$) and the reduced masses of the species ($\mu(i)$). Thus

$$\Delta\nu^0 = \nu^0(2) - \nu^0(1) = \Delta G(2) - \Delta G(1) \quad (1)$$

where

$$\Delta G(i) =$$

$$(\omega_e'(i)(v'+1/2) - \omega_e''(i)(v''+1/2)) - (\omega_e x_e'(i)(v'+1/2)^2 - \omega_e x_e''(i)(v''+1/2)^2) \quad (2)$$

$$\omega_e(2) = \rho\omega_e(1) \quad (3a)$$

$$\omega_e x_e(2) = \rho^2\omega_e x_e(1) \quad (3b)$$

$$\rho = \sqrt{\frac{\mu(1)}{\mu(2)}} \quad (4)$$

Furthermore, the relationship between rotational constants of the two isotopologues can be sought through the equations

$$B(2) = \rho^2 B(1) \quad (5a)$$

$$D(2) = \rho^4 D(1) \quad (5b)$$

Based on Eqs. (1) – (4), band origins due to transitions from the $A^2\Delta$(v′= 0) state to high energy states, with comparable potential curves (hence similar vibrational constants) will be similar and within the observation region for same v′ in the upper states (i.e. v′= 0), whereas band origins for higher v′s of the upper states (v′= 1,2) will be significantly lower for CD than for CH. Furthermore, based on Eqs. (4) – (5) the rotational structure will appear more compact for CD than for CH.

Fig. 6(a) shows the REMPI spectrum of $CDBr_3$ for CD^+ ion detection in the one-photon region of 40 300 - 41 500 cm^{-1}. The spectrum shows weak but reproducible band structures, largely irregular in shape. The band origin (ν^0) of the (2)$D^2\Pi$(v′= 2) spectrum for CD, based on the value of 41 023 cm^{-1} for CH was estimated, according to Eq. (1), to be about 39 726 cm^{-1} (Table 3), which is outside the observable and the energetically reachable region. It can, therefore, not account for the observed structure in the CD spectrum.

A spectral structure in the one-photon region of 41 030 – 41 175 cm^{-1} could be simulated (Fig. 6 (b) and Table 2(b)) by *Q* lines of a transition from the CD*($A^2\Delta$(v′= 0)) state to a CD**($^2\Pi$) state centered at ν^0 = 41 161.5 cm^{-1}. The simulation revealed some perturbations in the spectrum, showing as line-shifts as well as intensity alterations, which were accounted for by implementing an interaction with a $^2\Pi$ state, close in energy, (see

figure caption 6 (b)). Spectroscopic constants derived from the simulation are listed in Tables 3 and 4. Based on Eq. (1) the band origin for the corresponding CH spectrum, in the case of a v′= 0 state was estimated to be about 41 175 cm^{-1}. This value is i) -higher than that for the (2)$D^2\Pi$(v′= 2) spectrum, ii) -close to the upper part of the region of the uncertain spectral structure observed for CH (Fig. 2 (c)) and iii) -close to the origin of the spectrum assigned by J. Long *et al*.[14] to the $^2\Sigma^+$ state. We assign this spectrum to a transition to the $(4)^2\Pi$(v′= 0) state.

The band origin (ν^0) of the $(3)^2\Sigma^+$(v′= 0) spectrum for CD, judging from the work by Herzberg and Johns (see Table 4 and Ref.[29]) is about 41 346 cm^{-1}. Although the irregular and complicated band structure observed in the region of 41 280 – 41 480 cm^{-1} in the CD spectrum (Fig. 6 (a)) yet remains unassigned, we assign it to the $(3)^2\Sigma^+$(v′= 0) state. The perturbations of the spectral structure most probably are due to interactions with the $^2\Pi$ state(s), close in energy.

Finally, the remaining, irregular and seemingly perturbed structure, mainly observed on the low wavenumber side of the $(4)^2\Pi$(v′=0) spectrum for CD (Fig. 6 (a)), in the one-photon region of about 40 500 – 41 100 cm^{-1} could correspond to a spectrum in the range of about 40 410 – 41 090 cm^{-1} for CH**, v′= 0 state (see Table 3). The lower part of the region of the uncertain spectral structure observed for CH happens to be within that range. These structures we assign to the $(3)^2\Pi$(v′=0) state (see Table 3). The perturbations of the spectral structures most probably are due to interactions with the $^2\Pi$ states as well as the $^2\Sigma$ state, close in energy.

SUMMARY AND CONCLUSIONS

Mass resolved REMPI spectra for two-photon resonance excitations to Rydberg states of $CHBr_3$ were recorded and analysed for the excitation energy region of 76 000 – 84 000 cm^{-1}. Ion fragments, detected, were C^+, CH^+ and $^iBr^+$ (i = 79, 81) (Fig. 2 (a)).

The Br^+ spectra revealed number of Br(3/2) and Br*(1/2) ($2_r + 1_i$)REMPI atomic lines.[40]

The spectrum for C^+ showed, along with atomic lines,[40] a broad feature located at 80 666 cm^{-1}. This band, frequently observed in spectra of related compounds and which has been misinterpreted to be due to a molecular transition, is conclusively found to be associated with enhanced probability of ionization of C*($^1D_2$) fragments, when switching from three-photon to two-photon ionization. This conclusion shows that such effect need to be considered, carefully, when interpreting REMPI data in spectra analysis.

The CH^+ spectrum shows spectral features due to ($1_r + 1_i$)REMPI of CH*($A^2\Delta$(v′=0)) fragments in the one-photon resonance excitation region of about 40 370 – 41 380 cm^{-1}, (Fig.2 (b)). Analogous spectrum of CD^+ was also recorded for $CDBr_3$. Detailed analysis of both data sets revealed identification and assignment of spectra relevant to transitions to four high energy bound states for each fragment as well as characterization of some of the states as follows.

a) (2)$D^2\Pi$(v′= 2): CH: Majority of the band structure in the region of 40 450 – 41 150 cm^{-1} was assigned to *P*, *Q* and *R* line series of a transition to the (2)$D^2\Pi$(v′= 2) state (Fig. 2 (c)) and spectroscopic parameters were determined (Table 3) by simulations.[55] CD: As to be expected from isotope shift effects and the energetics relevant to the formation of the state, the spectrum does not appear.

b) $(3)^2\Sigma^+(v' = 0)$: CH: A weak signal detected near 41 314 cm^{-1} was assigned to the $(3)^2\Sigma^+(v' = 0)$ state (Fig. 2 (b)). CD: Band spectrum, showing large perturbation effects, in the regions of 41 280 – 41 480 cm^{-1} was assigned to the CD**$(3)^2\Sigma(v'= 0)$ state (Fig. 6 (a)).

c) $(4)^2\Pi(v'= 0)$: CH: Based on comparison with analysis of the CD spectrum some broad spectral features seen in the region of about 41 000 – 41 150 cm^{-1} are due to transitions to the $(4)^2\Pi(v'= 0)$ state. CD: Band spectrum, showing some slight perturbation effects, in the one-photon excitation region of 41 030 – 41 175 cm^{-1} was assigned to *Q* lines of a transition to the CD**($(4)^2\Pi(v'= 0)$) state (Fig. 6 (b)). Spectroscopic parameters were determined (Table 3) by simulation.[55]

d) $(3)^2\Pi(v'= 0)$: CH: Based on comparison with analysis of the CD spectrum some broad spectral features seen in the region of about 40 940 – 41 000 cm^{-1} are due to transitions to the $(3)^2\Pi(v'= 0)$ state. CD: Band spectrum, showing large perturbation effects, in the regions of 40 500 – 41 100 cm^{-1} was assigned to the CD**$(3)^2\Pi(v'= 0)$ state (Fig. 6 (a)).

Broad spectral lines observed, hence short lifetimes, are associated with predissociations by the repulsive $^2\Pi$ state. Whereas, the line widths of the broad spectra assigned to the $(3)^2\Pi(v'= 0)$ and $(4)^2\Pi(v'= 0)$ states for CH are particularly large, those of the $(2)D^2\Pi(v'= 2)$ spectrum for CH (4 - 6 cm^{-1}) and the $(4)^2\Pi(v'= 0)$ state for CD (1.5 – 3.5 cm^{-1}) also are relatively large, suggesting that predissociation of all the bound $^2\Pi$ states is of importance. Since such predissociation processes will form $C^*(^1D_2) + H$,[32] (see Fig. 2) it can, at least partly, explain the enhanced C^+, signal due to ionization of $C^*(^1D_2)$, mentioned before. Perturbations observed are associated with interactions between $^2\Pi$ and/or $^2\Sigma$ states in the energy region of concern.

The work on the data for the CH and CD fragments involved analysis of overlapping spectra of perturbed structure due to state interactions. Use of isotope shift effects as well as spectral simulations along with calculated potential surfaces[32, 33] was found to be necessary to clarify and characterise the states involved. Furthermore, this work demonstrates the usefulness of $(2_r + m_{r,i})$REMPI of parent molecules for molecular fragment analysis, where $m_{r,i} = 2$ (i.e. $m_{r,i} = 1_r + 1_i$) for CH* and CD* (i.e CH*/CD* $(1_r + 1_i)$REMPI).

ASSOCIATED CONTENT

Supporting Information

REMPI spectral lines for C/C* and Br/Br* atoms.

Acknowledgements

The financial support of the University Research Fund, University of Iceland and the Icelandic Science Foundation (Grant No. 130259-051) is gratefully acknowledged.

Figure captions:

Fig. 1. Schematic figure showing some important excitation and photofragmentation channels in (2_r + $m_{r,i}$)REMPI of CH_xBr_{4-x}; x = 2,3(see main text, INTRODUCTION). Unbroken vertical arrows are for resonance transitions, whereas broken vertical arrows represent non-resonance transitions. Non-vertical arrows represent dissociation paths for formation of neutral fragments (M, M*). M: ground state species, M*: valence molecular states or low energy excited states, M**: Rydberg states or high energy excited states, M^+: ionic states.

Fig. 2. $CHBr_3$:

(a) REMPI spectra for the ions C^+ (black), CH^+ (green) and Br^+(red) (below) for the two-photon excitation region 76 000 – 84 000 cm^{-1} (one-photon excitation region of 38 000 – 42 000 cm^{-1}) along with the absorption spectrum derived by Sander *et al*. (blue; top)[41]. The REMPI spectra are proportional in intensity. Markings (*) of atomic lines, seen in the Br^+ spectrum, indicate lines out of range.

(b) REMPI spectrum of $CHBr_3$ for the ion CH^+ for the two-photon excitation region of 80 600 – 82 800 cm^{-1} (one-photon region of 40 300 – 41 400cm^{-1}). Peaks marked with * are due to Coulomb broadening of C^+ signals. Spectral structures mainly and solely due to one-photon resonance excitations from CH*($A^2\Delta$(v′= 0)) to CH**((2)$D^2\Pi$(v′= 2)) and CH**((3)$^2\Sigma^+$(v′= 0)), respectively, are marked by horizontal black arrows for the spectral ranges and by vertical blue arrows for the band origins (v^0) (see Tables 3) . The vertical broken red arrow marks the band origin of the CH**((4)$^2\Pi$(v′= 0)) spectrum estimated from the corresponding CD** spectrum (see text and Table 3).

The inserted $(3)^2\Sigma^+(v'= 0)$ spectrum (above) was recorded for an increased laser power.

(c) Simulation of the CH*($A^2\Delta$ (v′= 0)) ($1_r + 1_i$)REMPI spectrum due to resonance transition to the $(2)D^2\Pi(v'= 2)$ state, derived by REMPI of $CHBr_3$ for CH^+ detection: Experimental spectrum (linewidths 4 – 6 cm^{-1}) at top (green), calculated spectrum for linewidths = 4 cm^{-1} in the middle (green) and *P* (red), *Q*(black) and *R*(red) lines at the bottom. Rotational line assignments are shown at top for the *N*′ numbers given in parenthesis. Peaks marked by * are due to Coulomb broadening of C^+ signals. Peaks and spectral features marked with # were not simulated. Simulation was carried out by using software package PGOPHER.[55] The top and bottom scales are the two- (2 hν) and one- (hν) photon wavenumbers, respectively.

The top and bottom scales, for all figures, are the two- (2 hν) and one- (hν) photon wavenumbers, respectively.

Fig. 3. $CHBr_3$, REMPI: Energetics, excitation and photofragmentation processes in REMPI of $CHBr_3$. The shaded area is the scanning region dealt with in this paper. The relative one-photon absorption intensity of $CHBr_3$ [1, 41] is tilted to the left (blue). For M = molecular or fragment species, M represent ground state species, M* are valence molecular states or low energy excited states, M** are Rydberg states or high energy excited states and M^+ are ionic states. Threshold energies (see Table 1) for CH/CH*/CH**/CH^+ and C/C*/C**/C^+ fragment formations and simultaneous Br and Br_2 formations, as well as relevant excitations and ionizations are indicated. Some 40 333 cm^{-1} (one-photon) / 80 666 cm^{-1} (two-photon) excitations are shown.

Fig. 4. C^+ REMPI for C^+ as a function of one- (bottom) and two- (top) photon excitation wavenumber for CH_xBr_{4-x}; x = 0 – 3, and $CDBr_3$ showing broad peaks centered at about 80 666 cm^{-1}, on the two-photon wavenumber scale. The broad peaks have been normalized to the same height and are highlighted by broken curves to guide the eye. The peaks are attributed to an enhanced non-resonance photoionization probability associated with switching from three-photon to two-photon ionization of $C^*(^1D_2)$ formed by two-photon dissociation of the parent molecules. The threshold for the two-photon ionization of $C^*(^1D_2)$ is indicated. Spectral bands surrounding the broad peak for CH_3Br are due to transitions to the parent molecular Rydberg states.[13]

Fig. 5.

$^2\Pi$ states potentials (black) and the $(3)^2\Sigma^+$ state potential (green) of CH** reproduced with permission from J. Chem. Physics, **126**, 164302, (2007) [33] and the authors (Vázquez *et al.*). Copyright 2007, AIP Publishing LLC. The coloured curves (blue, yellow, purple and red) represent our extrapolations and guesses for the diabatic curves of the states indicated ($(2)D^2\Pi$, $(3)^2\Pi$, $(4)^2\Pi$ and the repulsive $^2\Pi$ state).

Fig. 6.

a) REMPI spectrum of $CDBr_3$ for the ion CD^+ (green; top) for the two-photon excitation region of 80 600 – 83 000 cm^{-1} (one-photon region of 40 300 – 41 500 cm^{-1}) along with the CH^+ spectrum for $CHBr_3$ from Fig. 3(b)(faint grey; bottom). Peak marked by * is due to Coulomb broadening of a C^+ signal. The main spectral features due to transitions from $CD^*(A^2\Delta(v'= 0))$ to $CD^{**}((3)^2\Pi(v'= 0))$, $CD^{**}((4)^2\Pi(v'= 0))$ and

CD**($(3)^2\Sigma^+$(v′= 0)) are indicated by black horizontal arrows. Vertical blue arrows mark the band origins (ν^0) for the $(4)^2\Pi$(v′= 0) and $(3)^2\Sigma^+$(v′= 0) spectra (see Table 3).

b) Simulation of the CH*($A^2\Delta$; v′= 0) ($1_r + 1_i$)REMPI spectrum due to the resonance transition to the $(4)^2\Pi$(v′= 0) state derived by REMPI of $CDBr_3$ for CD^+ detection. Experimental spectrum (linewidth 1.5 – 3.5 cm^{-1}) at top (green), Calculated spectrum (linewidths = 1.5 cm^{-1}) in the middle (green) and *P* (red) and *Q* (black) lines at the bottom. Rotational line assignments are shown at top for the *N*′ numbers given in parenthesis. Perturbation effect, observed for *N*'= 3 – 6, appear as line shifts or intensity alterations. A homogenous perturbation from a nearby $^2\Pi$ state for N′~ 6 needed to be assumed in order to account for the spectral structure in that region.

The top and bottom scales, for both figures, are the two- (2 hν) and one- (hν) photon wavenumbers, respectively.

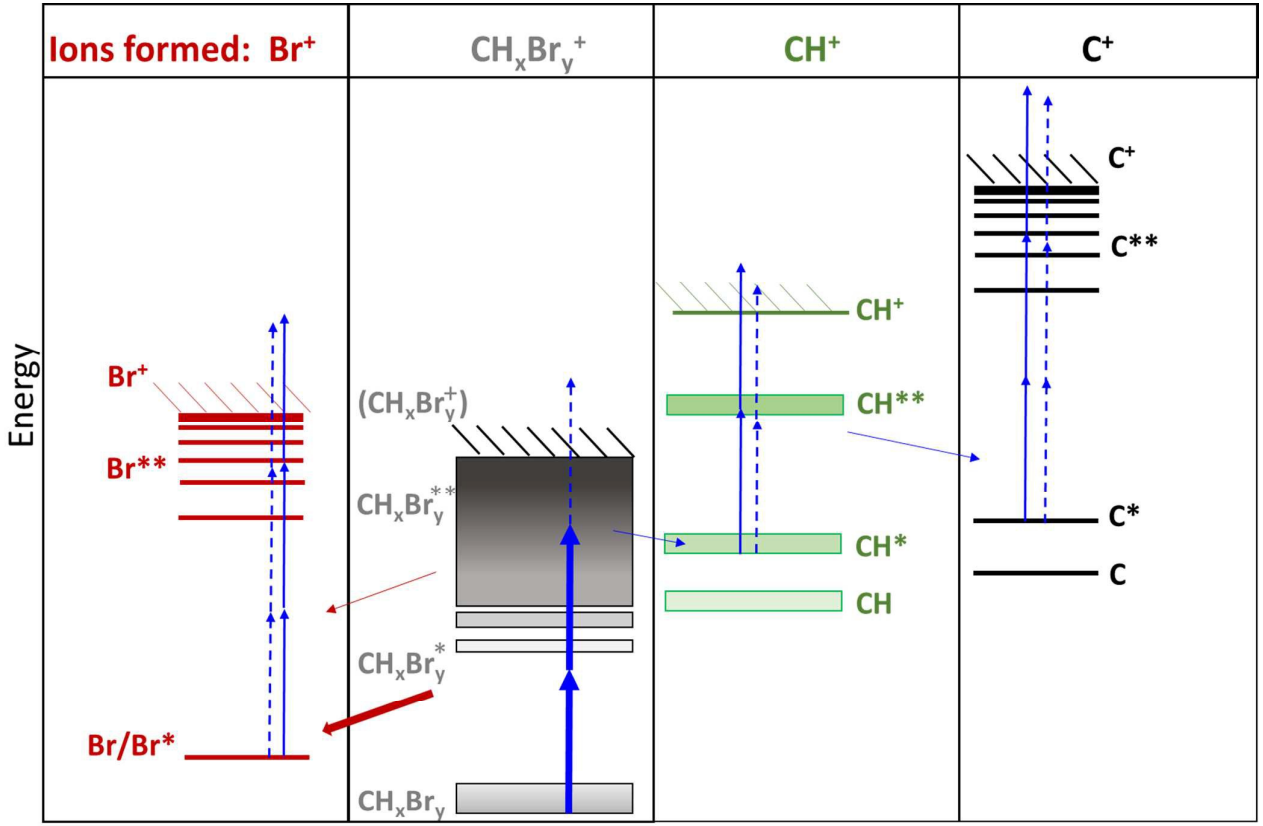

Fig. 1

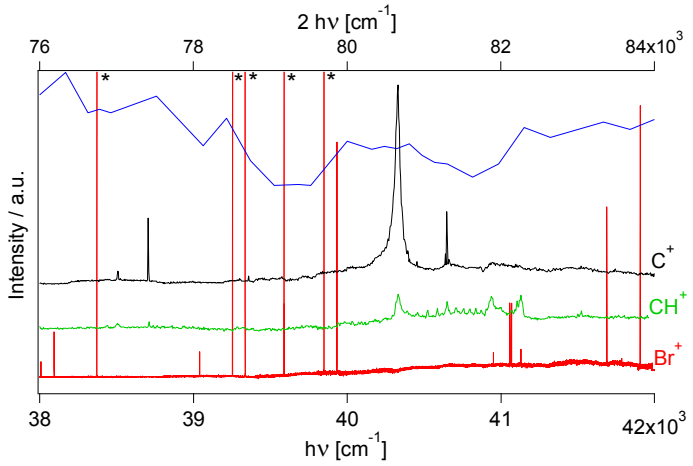

Fig. 2 (a)

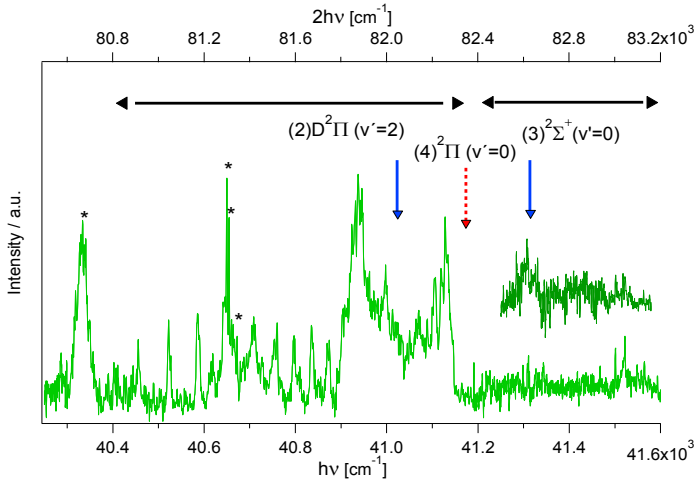

Fig. 2 (b)

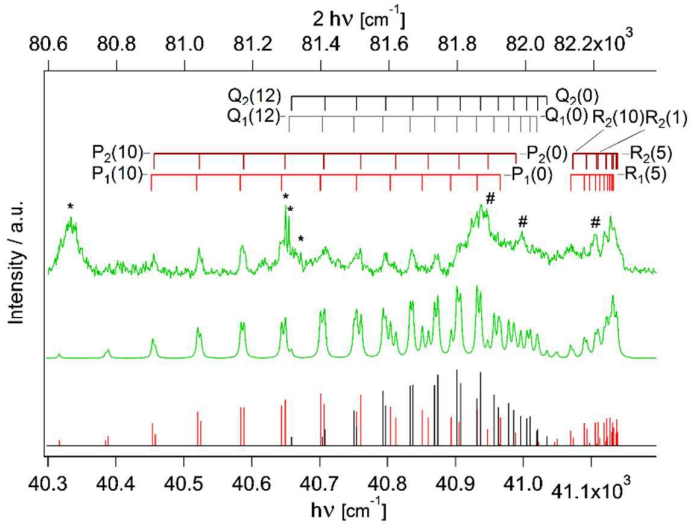

Fig. 2 (c)

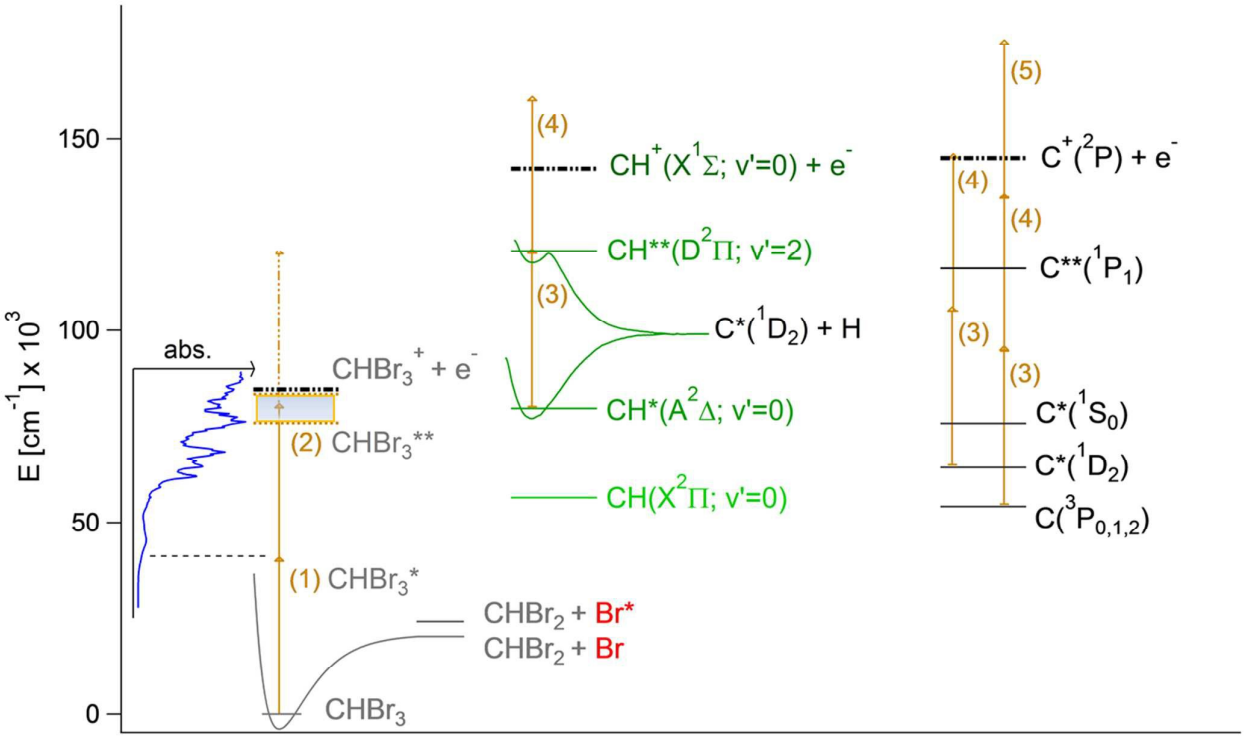

Fig. 3

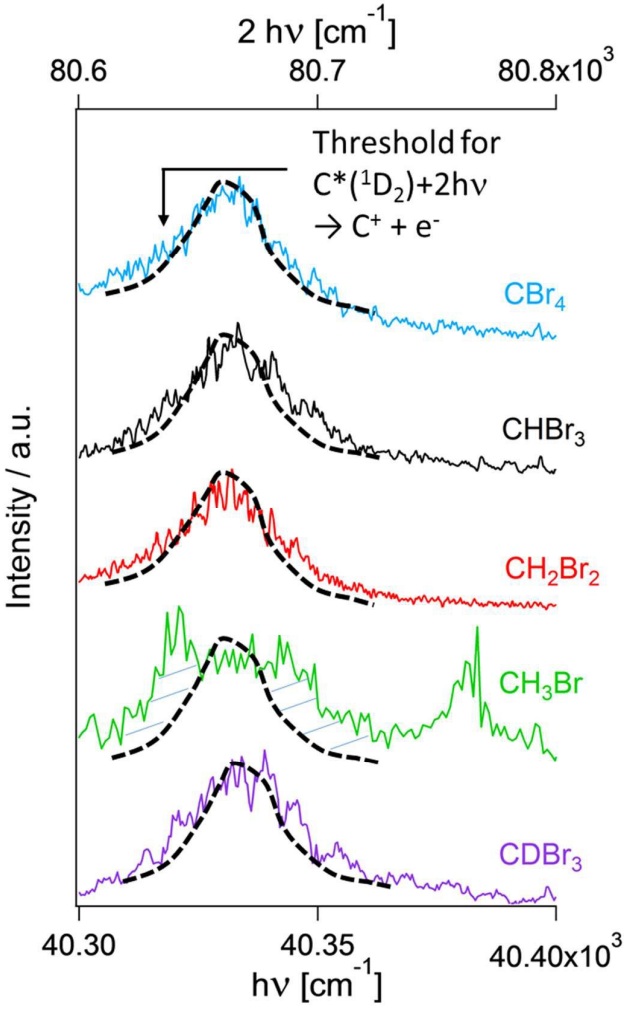

Fig. 4

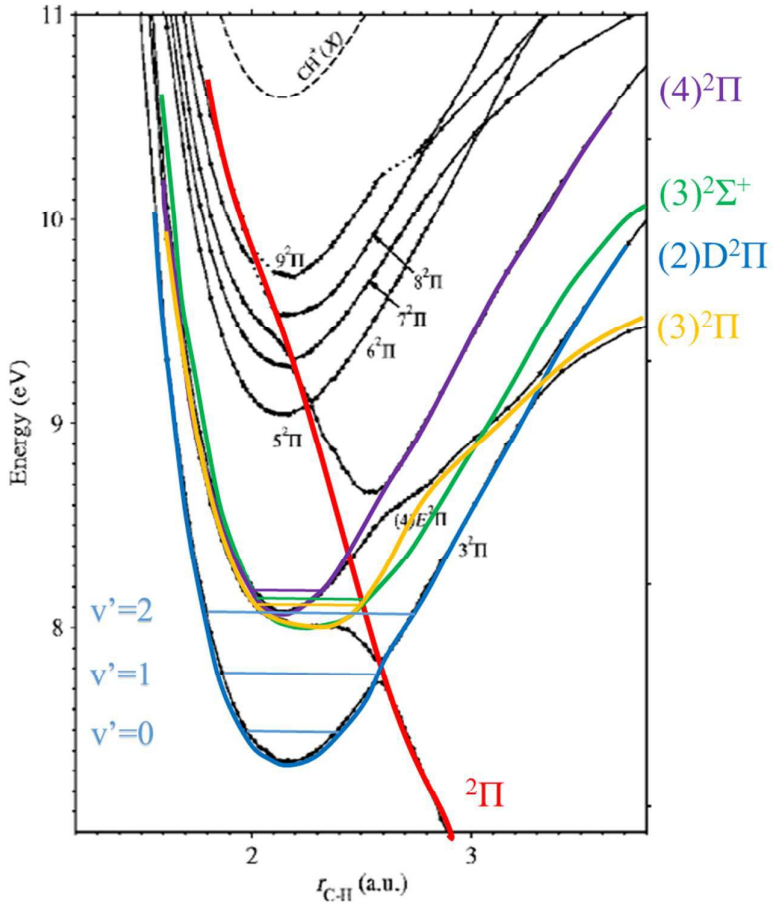

Fig. 5

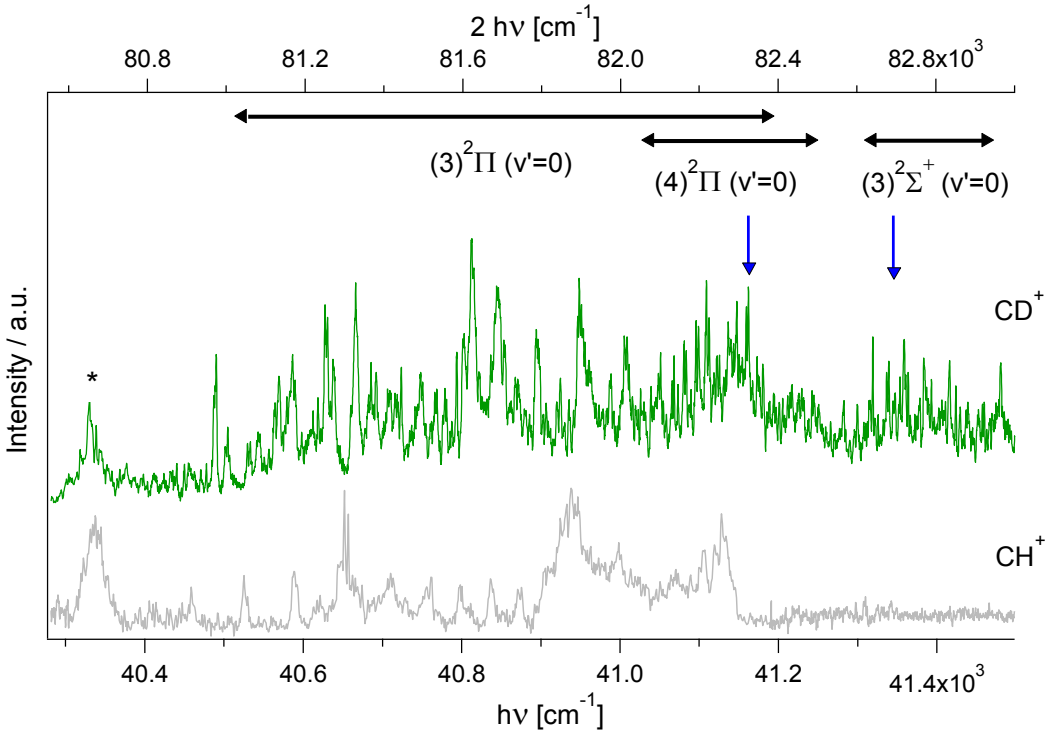

Fig. 6 (a)

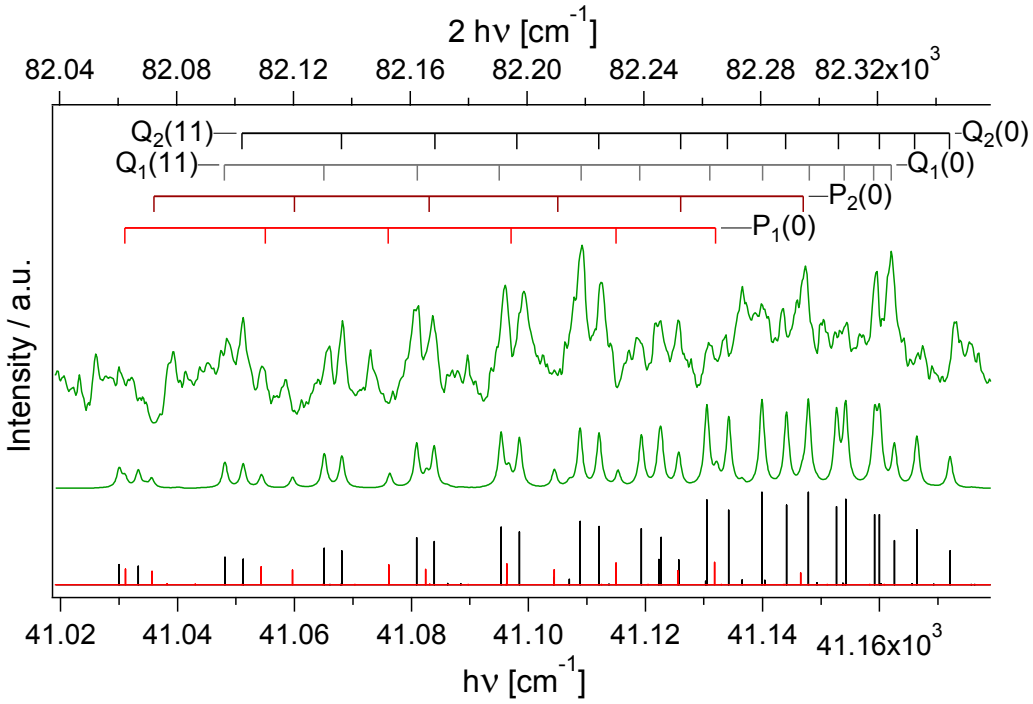

Fig. 6 (b)

Table 1. Energy thresholds (in wavenumbers / cm^{-1}) for fragmentations of $CHBr_3$. a) -within the observation region (76000 – 84000 cm^{-1}), b) -below the observation region.

	C / C*	CH/CH*	Br/Br*	Other fragments	Wavenumbers/ cm^{-1} [a]
a)	-	$CH(X^2\Pi)$	3 Br*(1/2)	-	83806.9
	-	$CH^*(A^2\Delta)$	Br*(1/2)	Br_2	83408.3
	$C^*(^1D_2)$	-	2 Br(3/2)	HBr	80636.7
	-	$CH(X^2\Pi)$	Br(3/2) , 2 Br*(1/2)	-	80121.7
	-	$CH^*(A^2\Delta)$	Br(3/2)	Br_2	79723.1
	$C(^3P_2)$	-	2 Br*(1/2)	HBr	77857.9
	$C(^3P_1)$	-	2 Br*(1/2)	HBr	77830.9
	$C(^3P_0)$	-	2 Br*(1/2)	HBr	77814.5
	-	$CH(X^2\Pi)$	2 Br(3/2) , Br*(1/2)	-	76436.4
b)	$C^*(^1S_0)$	-	-	HBr , Br_2	75874.9
	$C(^3P_2)$	-	Br(3/2) , Br*(1/2)	HBr	74172.7
	$C(^3P_1)$	-	Br(3/2) , Br*(1/2)	HBr	74145.7
	$C(^3P_0)$	-	Br(3/2) , Br*(1/2)	HBr	74129.3
	-	$CH(X^2\Pi)$	3 Br(3/2)	-	72751.2
	$C(^3P_2)$	-	2 Br(3/2)	HBr	70487.4
	$C(^3P_1)$	-	2 Br(3/2)	HBr	70460.4
	$C(^3P_0)$	-	2 Br(3/2)	HBr	70444.0
	$C^*(^1D_2)$	-	-	HBr, Br_2	64419.5
	-	$CH(X^2\Pi)$	Br*(1/2)	Br_2	60219.3
	-	$CH(X^2\Pi)$	Br(3/2)	Br_2	56534.1
	$C(^3P_2)$	-	-	HBr, Br_2	54270.3
	$C(^3P_1)$	-	-	HBr, Br_2	54243.3
	$C(^3P_0)$	-	-	HBr, Br_2	54226.9
	-	-	Br*(1/2)	$CHBr_2$	24147.5
	-	-	Br(3/2)	$CHBr_2$	20462.3

a. Values derived from bond energies [56, 57]

Table 2.

a) $CHBr_3$: CH*($A^2\Delta$(v′= 0)) ($1_r + 1_i$)REMPI rotational lines due to transitions to the (2)$D^2\Pi$(v′= 2) state derived from simulation calculations (cm^{-1}) [a]

N'	P_2	P_1	Q_2	Q_1	R_2	R_1
0	*40989*	*40966*	*41034*	*41020*		
1	*40948*	*40932*	*41021*	*41010*	*41108*	*41097*
2	*40905*	*40893*	*41005*	*40996*	*41121*	*41112*
3	*40860*	*40851*	*40986*	*40978*	*41130*	*41123*
4	*40812*	*40804*	*40963*	*40956*	*41136*	*41130*
5	40761	40754	*40937*	*40931*	*41139*	*41133*
6	40706	40701	*40907*	*40902*	*41137*	*41132*
7	40649	40644	40874	40869	*41132*	*41127*
8	40588	40583	40837	40833	*41123*	*41118*
9	40523	40519	40797	40793	*41110*	*41106*
10	40456	40452	40754	40750	*41093*	*41089*
11			*40707*	*40704*	*41073*	*41069*
12			*40658*	*40655*		

a. Roman type numbers are observable non-overlapped lines. Italic type numbers are overlapped lines.

Table 2.

b) $CDBr_3$: CD*($A^2\Delta$ (v′= 0)) ($1_r + 1_i$)REMPI rotational lines due to transitions to the (4)$^2\Pi$(v′= 0) state derived from simulation calculations (cm^{-1}) [a]

N'	P_2	P_1	Q_2	Q_1
0	*41147*	*41132*	41172	41162
1	*41126*	*41115*	41166	41159
2	*41105*	*41097*	*41160*	*41154*
3	*41083*	41076	*41153*	*41148*
4	41060	41055	*41144*	*41140*
5	*41036*	*41031*	*41134*	*41131*
6	*41010*	*41007*	41126	41119
7			41112	41109
8			41098	41095
9			41084	41081
10			41068	41065
11			*41051*	*41048*

a. Roman type numbers are observable non-overlapped lines. Italic type numbers are overlapped lines.

Table 3. Energetics and spectroscopic parameters for the CH** and CD** states (2)$D^2\Pi$(v′= 2), $(3)^2\Pi$(v′= 0), $(4)^2\Pi$(v′= 0) and $(3)^2\Sigma^+$(v′= 0) (cm^{-1}).

	$(2)D^2\Pi$ (v'=2) [a]		$(3)^2\Pi$ (v'=0) [b]		$(4)^2\Pi$ (v'=0) [c]		$(3)^2\Sigma^+$ (v'=0) [d]	
	CH	CD	CH	CD	CH	CD	CH	CD
ν^0 [e]	41023	39726	(40410-41090)	(40500-41100)	41175	41161	41314	41339
$T_{v',0}$ [e]	64196	62951	(63584-64264)	(63725-64325)	64348	64386	64531	64564
$B_{v'}$	12.74	6.87			13.41	7.23		
$D_{v'}$	0.00155	0.000451			0.00129	0.000375		
$H_{v'}$	7.5e-7							
A	-28.75					-19.4		
p [f]						-0.4		
q [f]						0.008		

a. CH values derived by a simulation[55] of the CH* ($A^2\Delta$ (v′= 0)) (1 + 1)REMPI spectrum for $CHBr_3$ for known parameters for the A state[58]; CD values derived from the corresponding CH values by Eqs. (1) – (5) and vibrational parameters from Refs.[33] (see also Table 4)

b. Ranges for CD estimated from the CD*($A^2\Delta$(v′= 0)) (1 + 1)REMPI spectrum (Fig. 5). Ranges for CH roughly estimated from the values for CD and Eqs. (1) – (5).

c. CD values derived by a simulation[55] of the CD*($A^2\Delta$(v′= 0)) (1 + 1)REMPI spectrum for $CDBr_3$ for known parameters for the A state[29, 59]; CH values derived from the corresponding CD values by Eqs. (1) – (5) and vibrational parameters from Refs.[33] (see also Table 4)

d. CH and CD values from Herzberg and Johns.[29]

e. $T_{v',0} = T_{v',0}(A^2\Delta(v'=0)) + \nu^0$; CH: $T_{v',0}(A^2\Delta(v'=0)) = 23173 cm^{-1}$ for footnotes (a)-(c)[58] and ; $T_{v',0}(A^2\Delta(v'=0)) = 23217 cm^{-1}$ for (d)[29]. CD: $T_{v',0}(A^2\Delta(v'=0)) = 23225\ cm^{-1}$ for (a)-(d)[59].

f. Λ-doubling parameters

Table 4. Summary of spectroscopic parameters (cm^{-1}) for the CH** states $(2)D^2\Pi(v'=2)$, $(3)^2\Pi(v'=0)$, $(4)^2\Pi(v'=0)$ and $(3)^2\Sigma^+(v'=0)$. ν^0 are band origins for transitions from the $A^2\Delta(v'=0)$ state. $T_{v',0}$ are energies of the v′ levels with respect to the ground state ($X^2\Pi$; v′′= 0). Electron configuration for short internuclear distances are specified.[33]

Terms and configuration		Dishoeck [a] *et al.*[32]	Kalemos [a] *et al.*[60]	Vázquez [a] *et al.*[33]	Herzberg [b] *et al.*[29]	Y.Chen [c] *et al.*[36]	Long [c] *et al.*[14]	Hafliðason [c] *et al.*
$(3)^2\Sigma^+$ (v'=0)	ν^0 [e, d]	*40004.6*	41903.5	40576.2	41314.0		41155.0	41314.0
$2s\sigma^2 2p\sigma^2 3p\sigma^1$	$T_{v',0}$ [e, d]	*64200.9*	65321.1	64006.9	64531.5		64328.0	64531.5
	ω_e		2475.1	2373.3				
	$\omega_e x_e$		147.27	50.77				
	B_v				12.17			
$(4)^2\Pi$ (v'=0)	ν^0 [e, d]	*40730.5*		41750.8				41101.0
$2s\sigma^2 2p\sigma^2 3p\pi^1$	$T_{v',0}$ [e, d]	*64926.8*		65181.5				64318.5
	ω_e			2996.2				
	$\omega_e x_e$			37.0-57.0				
$(3)^2\Pi$ (v'=0)	ν^0 [e, d]	*39842.3*	*40088.0*	*39881.8*		40427.0	40762.0	
$2s\sigma^2 2p\sigma^1 2p\pi^1 2p\sigma^1$*	$T_{v',0}$ [e, d]	*64039.6*	*63505.6*	*63312.5*		63600.0	63935.0	
$(2)D^2\Pi$ (v'=2)	ν^0 [e, d]		41016.7	41021.9	41038.2	40991.5	40991.5	41022.5
$2s\sigma^2 2p\pi^3$	$T_{v',0}$ [e, d]		64434.3	64452.6	64211.7	64165.0	64165.0	64196.0
	ω_e		2743.0	2781.1				
	$\omega_e x_e$		57.63	52.16				
	B_v				12.6	12.6	12.7	12.74
	D_v					0.00158	0.00158	0.00155
	A				-28.5	-26.6		-28.75

a.Calculated parameters; b.Experimental observations. $T_{v',0} = T_{v',0}(A^2\Delta\ (v'=0)) + \nu^0$; $T_{v',0}(A^2\Delta(v'=0))$ from Herzberg *et al.*[29]

c.Experimental values. $T_{v',0} = T_{v',0}(A^2\Delta(v'=0)) + \nu^0$; $T_{v',0}(A^2\Delta(v'=0))$ from Bernath *et al.*[58]

d.Roman type numbers are based on vibrational level energies; e.Italic type numbers are estimated from potential energy curves.

References:

1. G. C. Causley and B. R. Russell, *Journal of Chemical Physics*, 1975, **62**, 848-857.
2. S. Felps, P. Hochmann, P. Brint and S. P. McGlynn, *J. Molecular Spectroscopy*, 1976, **59**, 355-379.
3. G. N. A. Van Veen, T. Baller and A. E. De Vries, *Chemical Physics*, 1985, **92**, 59-65.
4. W. P. Hess, D. W. Chandler and J. W. Thoman, *Chemical Physics*, 1992, **163**, 277-286.
5. T. Gougousi, P. C. Samartzis and T. N. Kitsopoulos, *Journal of Chemical Physics*, 1998, **108**, 5742-5746.
6. D. D. Xu, J. H. Huang, R. J. Price and W. M. Jackson, *Journal of Physical Chemistry A*, 2004, **108**, 9916-9923.
7. R. Locht, B. Leyh, H. W. Jochims and H. Baumgartel, *Chemical Physics*, 2005, **317**, 73-86.
8. R. Locht, B. Leyh, D. Dehareng, H. W. Jochims and H. Baumgartel, *Chemical Physics*, 2005, **317**, 87-102.
9. R. Locht, B. Leyh, D. Dehareng, K. Hottmann, H. W. Jochims and H. Baumgartel, *Chemical Physics*, 2006, **323**, 458-472.
10. T. Ridley, J. T. Hennessy, R. J. Donovan, K. P. Lawley, S. Wang, P. Brint and E. Lane, *Journal of Physical Chemistry A*, 2008, **112**, 7170-7176.
11. V. Blanchet, P. C. Samartzis and A. M. Wodtke, *Journal of Chemical Physics*, 2009, **130**.
12. F. Y. Wang, M. L. Lipciuc, X. M. Yang and T. N. Kitsopoulos, *Physical Chemistry Chemical Physics*, 2009, **11**, 2234-2240.
13. K. Matthiasson, Á. Kvaran, H. Wang and A. Bodi, *Journal of Physical Chemistry A*, 2010, **114**, 9991-9998.
14. J. Long, H. Wang and Á. Kvaran, *The Journal of Physical Chemistry A*, 2014, **118**, 1826-1831.
15. Y. L. Yung, J. P. Pinto, R. T. Watson and S. P. Sander, *Journal of Atmospheric Sciences*, 1980, **37**, 339-353.
16. M. J. Prather and R. T. Watson, *Nature*, 1990, **344**, 729-734.
17. R. von Glasow, R. von Kuhlmann, M. G. Lawrence, U. Platt and P. J. Crutzen, *Atmospheric Chemistry and Physics*, 2004, **4**, 2481-2497.
18. J. I. Lunine, *Astrobiology*, Pearson - Addison-Wesley 2005.
19. P. Ehrenfreund and M. A. Sephton, *Faraday Discussions*, 2006, **133**, 277-288.

20. N. J. Warwick, J. A. Pyle and D. E. Shallcross, *Journal of Atmospheric Chemistry*, 2006, **54**, 133-159.
21. J. Aschmann and B.-M. Sinnhuber, *Atmospheric Chemistry and Physics*, 2013, **13**, 1203-1219.
22. K. A. Peterson and J. S. Francisco, *Journal of Chemical Physics*, 2002, **117**, 6103-6107.
23. P. Zou, J. Shu, T. J. Sears, G. E. Hall and S. W. North, *Journal of Physical Chemistry*, 2004, **108**, 1482-1488.
24. A. M. Shaw, *Astrochemistry; From Astronomy to Astrobiology*, Wiley 2006.
25. D. Gillotay, P. C. Simon and L. Dierickx, *Aeronomica Acta A*, 1988, **335**, 1-25.
26. D. A. Gillotay, B. Jenouvrier, B. Coquert, M. F. Merienne and P. C. Simon, *Planet Space Sci*, 1989, **37**, 105-108.
27. T. Munakata and T. Kasuya, *Chemical Physics Letters*, 1989, **154**, 604-609.
28. R. Locht, B. Leyh, H. W. Jochims and H. Baumgartel, *Chemical Physics*, 2005, **317**, 73-86.
29. G. Herzberg and J. W. C. Johns, *The Astrophysical Journal*, 1969, **158**, 399-418.
30. P. Chen, W. A. Chupka and S. D. Colson, *Chemical Physics Letters*, 1985, **121**, 405-407.
31. P. Chen, J. B. Pallix, W. A. Chupka and S. D. Colson, *The Journal of Chemical Physics*, 1987, **Vol 86**, 516-520.
32. E. F. van Dishoeck, *Journal of Chemical Physics*, 1986, **86**, 196-214.
33. G. J. Vázquez, J. M. Amero, H. P. Liebermann, R. J. Buenker and H. Lefebvre-Brion, *Journal of Chemical Physics*, 2007, **126**, 164302-164313.
34. P. J. H. Tjossem and C. Smyth, *Chemical Physics Letters*, 1987, **144**, 51-57.
35. Y. Wang, L. Li and W. A. Chupka, *Chemical Physics Letters*, 1992, **192**, 348-352.
36. Y. Chen, J. Jin, L. Pei, X. Ma and C. Chen, *Journal of Electron Spectroscopy and Related Phenomena*, 2000, **108**, 221-224.
37. K. Matthiasson, J. Long, H. Wang and Á. Kvaran, *Journal of Chemical Physics*, 2011, **134**, 164302.
38. J. Long, H. Wang and Á. Kvaran, *Journal of Chemical Physics*, 2013, **138**, 044308.
39. K. Matthiasson, H. Wang and Á. Kvaran, *Chemical Physics Letters*, 2008, **458**, 58-63.
40. See Supporting Information.

41. S. P. Sander, J. Abbatt, J. R. Barker, J. B. Burkholder, R. R. Friedl, D. M. Golden, R. E. Huie, C. E. Kolb, M. J. Kurylo, G. K. Moortgat, V. L. Orkin and P. H. Wine, *JPL Publication*, 2011, **10-6**.
42. B. G. Waage, Á. Kvaran and H. Wang, *Journal of Chemical Physics*, 2000, **113**, 1755-1761.
43. Á. Logadóttir, Á. Kvaran and H. Wang, *Journal of Chemical Physics*, 2000, **112**, 10811-10820.
44. J. Long, Á. Kvaran, K. Sveinbjörnsson and H. Wang, *Chemical Physics Letters*, 2011, **516**, 12-16.
45. H. M. Lambert, P. J. Dagdigian and M. H. Alexander, *Journal of Chemical Physics*, 1998, **108**, 4460-4466.
46. Y.-L. He and D. Wang, *Structural Chemistry*, 2009, **20**, 461-479.
47. P. Chen, J. B. Pallix, W. A. Chupka and S. D. Colson, *Journal of Chemical Physics*, 1986, **84**, 5208-5209.
48. Á. Logadóttir, Á. Kvaran and H. Wang, *Journal of Chemical Physics*, 1998, **109**, 5856-5867.
49. Á. Kvaran and H. Wang, *Journal of Molecular Spectroscopy*, 2004, **228**, 143-151.
50. K. Matthiasson, Á. Kvaran, H. Wang, A. Bodi and E. Jónsson, *Journal of Chemical Physics*, 2008, **129**, 164313.
51. K. Matthiasson, Á. Kvaran and H. Wang, *Journal of Chemical Physics*, 2009, **131**, 044324.
52. K. Matthiasson, Á. Kvaran and H. Wang, *Journal of Molecular Spectroscopy*, 2009, **255**, 1-5.
53. H. R. Hróðmarsson, H. Wang and Á. Kvaran, *Journal of Molecular Spectroscopy*, 2013, **290**, 5-12.
54. H. R. Hróðmarsson, H. Wang and Á. Kvaran, *Journal of Chemical Physics*, 2014, **140**, 244304.
55. C. M. Western, *PGOPHER, a Program for Simulating Rotational Structure, C. M. Western, University of Bristol,* http://pgopher.chm.bris.ac.uk University of Bristol 2003-2015.
56. V. Chikan, F. Fournier and S. R. Leone, *Journal of Chemical Physics*, 2006, **110**, 2850-2857.
57. W. M. Haynes and D. R. Lide, *CRC handbook of chemistry and physics: A ready-reference book of chemical and physical data*, CRC, Boca Raton, Fl, 2010.

58. P. F. Bernath, C. R. Brazier, T. Olsen, R. Hailey, W. T. M. L. Fernando, C. Woods and J. L. Hardwick, *Journal of Molecular Spectroscopy*, 1991, **147**, 16-26.

59. "Constants of diatomic molecules", NIST Chemistry WebBook, http://webbook.nist.gov/cgi/cbook.cgi?ID=C13776700&Units=SI&Mask=1000, Accessed October 2015.

60. A. Kalemos, A. Mavridis and A. Metropoulos, *Journal of Chemical Physics*, 1999, **111**, 9536-9548.